Pergamon

Int. J. Heat Mass Transfer. Vol. 40, No. 13, pp. 3105–3117, 1997

Printed in Great Britain
0017-9310/97 $17.00 + 0.00

PII: S0017-9310(96)00352-3

Laminarization of turbulent gas flow inside a strongly heated tube

SHUICHI TORII
Department of Mechanical Engineering, Kagoshima University, 1-21-40 Korimoto, Kagoshima 890, Japan

and

WEN-JEI YANG†
Department of Mechanical Engineering and Applied Mechanics, University of Michigan, Ann Arbor, MI 48109, U.S.A.

(*Received* 2 *April* 1996 *and in final form* 8 *October* 1996)

Abstract—A numerical study is performed to investigate thermal transport phenomena of the laminarizing flow in a strongly heated circular tube. A k–ε turbulence model is employed to determine the turbulent viscosity and the turbulent kinetic energy. The turbulent heat flux is expressed by Boussinesq approximation in which the eddy diffusivity for heat is determined by a $t^2-\varepsilon_t$ heat-transfer model. Both models are slightly modified to improve the accuracy in the turbulent-to-laminar transition region. The governing boundary layer equations are discretized by means of a control volume finite-difference technique and numerically solved using a marching procedure. Results are obtained for Stanton number, turbulent kinetic energy, temperature variance and velocity and temperature dissipation time scales in laminarizing flow. © 1997 Elsevier Science Ltd.

INTRODUCTION

When a gas in a channel is heated with extremely high heat flux, the flow may be laminarized. So-called laminarization implies that a strongly heated gas flow, which is certainly turbulent at the entrance of the channel, exhibits heat transfer characteristics of laminar flows in the down stream part. That is, a transition from turbulent to apparent laminar flow, occurs at higher Reynolds number than the usual critical value. Both the proposed criteria for the occurrence of laminarization and the heat transfer characteristics of this phenomenon have been reported by several investigators [1–6]. It is commonly accepted that: (i) some locally defined Reynolds numbers, such as a turbulent Reynolds number, are remarkably reduced, particularly in the vicinity of the heated wall; and (ii) this is caused by the effect of acceleration due to gas expansion, resulting in laminarization. Experimental data [1–6] are found in the literature as to the bulk flow properties such as heat transfer coefficients or pressure drops along the stream. Moreover, radial distributions of the time-averaged velocity and temperature near the entrance region are also measured by Mori and Watanabe [5] and Perkins and McEligot [7], respectively. However, to the authors' knowledge, there is no detailed experimental data pertinent to flow and thermal characteristics such as turbulence quantities in the laminarizing flow. This is because measurement of the turbulent quantities in strongly heated laminarizing flows is very difficult. Numerical simulation gives detailed information which furthers our understanding of the transport phenomena.

Kawamura [8], Torii *et al.* [9] and Fujii *et al.* [10] analyzed the laminarization phenomena in strongly heated gas flows by means of k–kL, k–ε and k–kL–$\overline{uv}$ models, respectively. They all revealed that turbulent kinetic energy is substantially attenuated in the vicinity of a heated wall, resulting in the remarkable reduction in heat transfer. Since the above three different turbulence models basically assume isotropic turbulence structure, they cannot precisely reproduce the anisotropy of turbulence caused by rapid flow acceleration due to gas expansion. In order to obtain detailed information on the flow structures, the higher order closure model, i.e. a Reynolds stress turbulence model is employed. Torii *et al.* [11] investigated transport phenomena in strongly heated circular tube flows by means of the Reynolds stress turbulence model of Launder and Shima [12]. It is disclosed that: (i) even when a substantial reduction in heat transfer, i.e. laminarization takes place, the turbulent kinetic energy does not disappear completely; and (ii) lami-

† Author to whom correspondence should be addressed.

NOMENCLATURE

c_p specific heat at constant pressure [J (kgK)$^{-1}$]
C_μ, C_1, C_2 empirical constants of k–ε model
C_λ, C_{P1}, C_{P2}, C_{D1}, C_{D2} turbulence model constants for temperature field
D diameter [m]
f friction coefficient
f_μ, f_1, f_2 turbulence model functions of k–ε model
f_λ, f_{P1}, f_{P2}, f_{D1}, f_{D2} turbulence model functions of temperature field
g acceleration of gravity [m s^{-2}]
G mass flux of gas flow [kg (m^{2}s)]
Gr Grashof number, $gq_wD^4(\nu^2\lambda T)_{in}$
h heat transfer coefficient [W m^{-2} K^{-1}]
k turbulent kinetic energy [m^2 s^2]
Nu Nusselt number, hD/λ
P time-averaged pressure [Pa]
Pr Prandtl number
Pr_t turbulent Prandtl number
q heat flux [W m^{-2}]
q_{in}^+ dimensionless heat flux parameter, $q_w/(Gc_pT)_{in}$
r radial coordinate [m]
R time-scale ratio, $R = \dfrac{t^2/2\varepsilon_t}{k/\varepsilon}$
Re Reynolds number, u_mD/ν
R_t turbulent Reynolds number, $k^2/(\varepsilon\nu)$
R_τ dimensionless distance in radial direction, $= y^\pm$
St Stanton number, $q_w/(\rho c_p u_m(T_w - T_b))$
T time-averaged temperature [K]
t fluctuating temperature component [K]
t^* friction temperature, $q_w/(\rho c_p u^*)$ [K]
$\overline{t^2}$ temperature variance [K^2]
U, V time-averaged velocity components in axial and radial directions, respectively [m s^{-1}]
$\hat{V}$ instantaneous velocity component in radial direction, $V+v$ [m s^{-1}]
u_m mean velocity over tube cross section, $u_m = \dfrac{8}{D^2}\displaystyle\int_0^{D/2} Ur\,dr$ [m s^{-1}]
u, v fluctuating velocity components in axial and radial directions, respectively [m s^{-1}]
u^* friction velocity, $\sqrt{\tau_w/\rho}$ [m s^{-1}]
x axial coordinate [m]
y distance from wall [m]
y^+ dimensionless distance, u^*y/ν.

Greek symbols
α_t turbulent thermal diffusivity [m^2 s^{-1}]
ρ density [kg m^{-3}]
ε turbulent energy dissipation rate [m^2 s^{-3}]
ε_t dissipation rate of $\overline{t^2}$ [K s^{-2}]
λ, λ_t molecular and turbulent thermal conductivities, respectively [W (Km)$^{-1}$]
μ, μ_t molecular and turbulent viscosities, respectively [Pa s]
ν fluid kinematic viscosity [m^2 s^{-1}]
σ_k, σ_ε, σ_h, σ_ϕ turbulence model constants for diffusion of k, ε, $\overline{t^2}$ and ε_t, respectively
τ_u, τ_t time scales of velocity and temperature fields, respectively, k/ε, $\overline{t^2}/(2\varepsilon_t)$ [s]
τ_w wall shear stress [Pa]
θ tangential direction
θ^+ dimensionless temperature, equation (18).

Subscripts
b bulk
c center
in inlet
max maximum
w wall.

Superscripts
$\bar{}$ time averaged value
$'$ fluctuation value
$\hat{}$ instaneous value.

narization due to strong heating, causes both a reduction in the Reynolds stress and an amplification of the inherent anisotropy of the turbulence structure. Koshizuka *et al.* [13] analyzed heat transfer characteristics at supercritical water cooling in a vertical pipe, by means of a k–ε model. They reported that heat transfer deterioration is caused by two mechanisms depending on the flow rate, i.e. an increase in viscosity near the wall by heating for the large flow rate and an acceleration of the flow velocity near the wall by buoyancy force of the small flow rate.

In the above numerical simulations pertinent to turbulent heat transport problems, the turbulent heat flux in the energy equation is modeled on the class Boussinesq approximation. The unknown thermal conductivity, λ_t, is obtained from the definition of the specific heat, c_p, the known turbulent viscosity, μ_t, and turbulent Prandtl number, Pr_t, as $\lambda_t = c_p\mu_t/Pr_t$.

However, calculation with this formulation gives no more detailed information on heat transport phenomena, such as temperature fluctuation and turbulent heat flux. To acquire this information, the one- and two-equation models for thermal field and the turbulent heat flux equation model are employed.

Nagano and Kim [14] proposed a two-equation model for thermal field, in which the temperature variance, $\overline{t^2}$ and the dissipation rate of temperature fluctuations, ε_t, are used together with k and ρ to model a thermal eddy diffusivity, α_t. This model, taking the near-wall behavior into account, was developed to investigate the heat transport phenomena under the uniform wall-temperature condition, resulting in better prediction accuracy for a flat-plate thermal boundary layer, the thermal entrance region of a pipe, and the turbulent heat transfer in fluids with different Prandtl numbers. Youssef *et al.* [15] modified the original two-equation heat-transfer model of Nagano and Kim [14] to reproduce the wall limiting behavior of turbulence quantities in a thermal field under arbitrary wall thermal conditions. Sommer *et al.* [16] derived a near-wall two-equation heat-transfer model similar to that of Nagano and Kim [14] and Youssef *et al.* [15], in which a Reynolds stress model is employed to ensure accuracy and reliability in the predicted velocity field. It was found by the authors' preliminary examination that (i) accuracy of the two-equation heat-transfer model of Nagano and Kim [14] is somewhat inferior to that of the other $\overline{t^2}$–ε_t heat-transfer models, particularly for heat transfer analysis under the uniform wall heat flux condition; and (ii) the former model, however, yields short computing times and more stable computations than the latter models because of its simplicity.

The purpose of the present study is to investigate the laminarization phenomena of a strongly heated gas flow in a circular tube, particularly heat transfer mechanism in the laminarizing flow. The two-equation model for heat transfer proposed by Nagano and Kim [14] and the k–ε turbulence model of Nagano and Hishida [17] are employed to determine the mechanism of the heat transport phenomena. A slight modification to both original models is made to improve their accuracy, particularly in the low-Reynolds-number region. The turbulent thermal conductivity, λ_t, is determined by using the temperature variance and the dissipation rate of temperature fluctuations together with k and ε. Emphasis is placed on streamwise variation of the flow and thermal fields in the laminarizing flow, particularly temperature profile, turbulent heat flux and temperature variance.

GOVERNING EQUATIONS

A turbulent flow in a strongly heated circular tube, as shown in Fig. 1, is analyzed using cylindrical coordinates. In this analysis, dependence of the gas properties on temperature, as well as the change in gas density, must be taken into account. The boundary

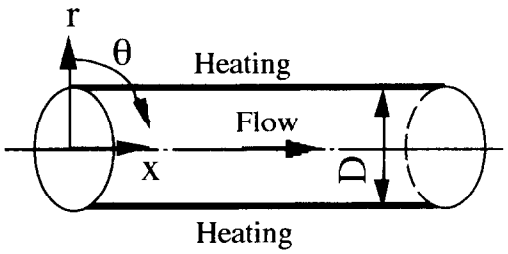

Fig. 1. A schematic of the physical system and coordinates.

layer approximation is employed to express the steady, two-dimensional, continuity, energy and momentum equations as

$$\frac{\partial(\bar{\rho}U)}{\partial x}+\frac{1}{r}\frac{\partial(r\overline{\rho\hat{V}})}{\partial r}=0 \tag{1}$$

$$c_p\bar{\rho}U\frac{\partial T}{\partial x}+c_p\overline{\rho\hat{V}}\frac{\partial T}{\partial r}=\frac{1}{r}\frac{\partial}{\partial r}\left(r\lambda\frac{\partial T}{\partial r}-rc_p\bar{\rho}\overline{vt}\right) \tag{2}$$

and

$$\bar{\rho}U\frac{\partial U}{\partial x}+\overline{\rho\hat{V}}\frac{\partial U}{\partial r}=-\frac{\mathrm{d}P}{\mathrm{d}x}+\frac{1}{r}\frac{\partial}{\partial r}\left(r\mu\frac{\partial U}{\partial r}-r\bar{\rho}\overline{uv}\right) \tag{3}$$

respectively. Here, the term for body force in the momentum equation was negligible, because a small diameter tube was employed and throughout the calculation, the buoyancy parameter, Gr/Re_{in}^2, was less than 0.1 so that the forced convection may be expected to dominate.

Using the turbulent conductivity, λ_t, the turbulent heat flux, $-c_p\bar{\rho}\overline{vt}$ in equation (2), is expressed by the following simple gradient form:

$$-c_p\bar{\rho}\overline{vt}=\lambda_t\frac{\partial T}{\partial r}. \tag{4}$$

Nagano and Kim [14] model λ_t in terms of the temperature variance, $\overline{t^2}$ and the dissipation rate of temperature fluctuations, ε_t, k and ε, as

$$\lambda_t=c_p\bar{\rho}C_\lambda f_\lambda k\sqrt{\frac{\overline{kt^2}}{\varepsilon\varepsilon_t}} \tag{5}$$

where C_λ is a model constant and f_λ is a model function. In the present study, the two-equation heat-transfer model developed by Nagano and Kim [14] is used to obtain $\overline{t^2}$ and ε_t in equation (5). The transport equations for $\overline{t^2}$ and ε_t are expressed as

$$\bar{\rho}U\frac{\partial\overline{t^2}}{\partial x}+\overline{\rho\hat{V}}\frac{\partial\overline{t^2}}{\partial r}=\frac{1}{r}\frac{\partial}{\partial r}\left\{r\left(\frac{\lambda_t}{c_p\sigma_h}+\frac{\lambda}{C_p}\right)\frac{\partial\overline{t^2}}{\partial r}\right\}+\frac{2\lambda_t}{C_p}\left(\frac{\partial T}{\partial r}\right)^2-2\rho\varepsilon_t-2\frac{\lambda}{c_p}\left(\frac{\partial\sqrt{\overline{t^2}}}{\partial r}\right)^2 \tag{6}$$

and

Table 1. Empirical constants and model functions in the $\overline{t^2}-\varepsilon_t$ heat-transfer model of Nagano and Kim [14]

$C\lambda$	C_{P1}	C_{P2}	σ_h	σ_ϕ	C_{D1}	C_{D2}	f_{P1}	f_{P2}	f_{D1}	f_{D1}	$f\lambda$
0.11	1.80	0.72	1.0	1.0	2.20	0.80	1.0	1.0	1.0	1.0	$\left\{1-\exp\left(-\frac{\sqrt{Pr}}{30.5}\frac{2}{f}Sty^+\right)\right\}^2$

$$\bar{\rho}U\frac{\partial\varepsilon_t}{\partial x}+\overline{\rho}\overline{V}\frac{\partial\varepsilon_t}{\partial r}=\frac{1}{r}\frac{\partial}{\partial r}\left\{r\left(\frac{\lambda_t}{c_p\phi}+\frac{\lambda}{c_p}\right)\frac{\partial\varepsilon_t}{\partial r}\right\}$$
$$+C_{P1}f_{P1}\frac{\lambda_t\varepsilon_t}{c_{p_t}\overline{2}}\left(\frac{\partial T}{\partial r}\right)^2+C_{P2}f_{P2}\mu_t\frac{\varepsilon_t}{k}\left(\frac{\partial U}{\partial r}\right)^2-C_{D1}f_{D1}\rho\frac{\varepsilon_t^2}{\overline{t^2}}$$
$$-C_{D2}f_{D2}\rho\frac{\varepsilon\varepsilon_t}{k}+\frac{\alpha\lambda_t}{c_p}(1-f_\lambda)\left(\frac{\partial^2T}{\partial r^2}\right)^2 \quad (7)$$

respectively. The empirical constants and model functions in equations (5), (6) and (7) are summarized in Table 1.

The Reynolds stress, $-\bar{\rho}\overline{uv}$, in equation (3) is obtained using the Boussinesq approximation as

$$-\bar{\rho}\overline{uv}=\mu_t\frac{\partial U}{\partial r}. \quad (8)$$

Here, the turbulent viscosity, μ_t, can be expressed in terms of the turbulent kinetic energy, k and its dissipation rate, ε, through the Kolmogorov–Prandtl's relation [18], as

$$\mu_t=\bar{\rho}C_\mu f_\mu\frac{k^2}{\varepsilon}. \quad (9)$$

C_μ and $f\mu$ are model constant and a model function, respectively. In determining $\overline{t^2}$ and ε_t in equation (5), Nagano and Kim [14] used the low Reynolds number version of a k–ε turbulence model developed by Nagano and Hishida [17]. The same model is employed here. The transport equations read

$$\bar{\rho}U\frac{\partial k}{\partial x}+\overline{\rho}\overline{V}\frac{\partial k}{\partial r}=\frac{1}{r}\frac{\partial}{\partial r}\left\{r\left(\frac{\mu_t}{\sigma_k}+\mu\right)\frac{\partial k}{\partial r}\right\}$$
$$+\mu_t\left(\frac{\partial U}{\partial r}\right)^2-\bar{\rho}\varepsilon-2\mu\left(\frac{\partial\sqrt{k}}{\partial r}\right)^2 \quad (10)$$

and

$$\bar{\rho}U\frac{\partial\varepsilon}{\partial x}+\overline{\rho}\overline{V}\frac{\partial\varepsilon}{\partial r}=\frac{1}{r}\frac{\partial}{\partial r}\left\{r\left(\frac{\mu_t}{\sigma\varepsilon}+\mu\right)\frac{\partial\varepsilon}{\partial r}\right\}$$
$$+C_1f_1\bar{\rho}\frac{\varepsilon}{k}\mu_t\left(\frac{\partial U}{\partial r}\right)^2-C_2f_2\frac{\varepsilon^2}{k}$$
$$+\nu\mu_t(1-f_\mu)\left(\frac{\partial^2U}{\partial r^2}\right)^2. \quad (11)$$

The empirical constants and model functions in equations (9), (10) and (11) are summarized in Table 2.

In the following, a combination of the k–ε turbulence model of Hagano and Hishida [17] and the two-equation heat-transfer model of Nagano and Kim [14] is designated as "Model A".

NUMERICAL SCHEME

A set of governing equations may be solved using the control volume finite-difference procedure developed by Patandar [19]. Since all turbulent quantities as well as the time-averaged streamwise velocity vary rapidly in the near-wall region, the size of non-uniform cross-stream grids is increased in a geometric ratio from the wall towards the center line. The maximum control volume size near the center line is always kept less 3% of tube radius. In order to ensure accuracy of the calculated results, at least two control volumes are located in the viscous sublayer, i.e. $y^+=5$. This is because the authors' preliminary examination disclosed that (i) if one control volume or no control volume is located in the viscous sublayer, the predicted Nusselt number does not agree with the experimental correlation for the slightly heated pipe flow case, and the temperature profile is not in accord with the law of the wall for the thermal field; and (ii) when two and five control volumes are located in $y^+=5$, there in no substantial difference between

Table 2. Empirical constants and model functions in the k–ε turbulence model of Nagano and Hishida [17]

C_μ	C_1	C_2	σ_k	σ_ε	f_1	f_2	f_μ
0.09	1.45	1.9	1.0	1.3	1.0	$1-0.3\exp(-R_t^2)$	$\left\{1-\exp\left(\frac{R_\varepsilon}{26.5}\right)\right\}^2$

both calculations for the strongly heated pipe flow cases. Throughout our numerical calculations, the number of control volumes is properly selected between 62 and 98 to obtain a grid-independent solution, resulting in no appreciable difference between the numerical results with different grid spacing. The discretized equations are solved from the inlet along the flow direction by means of a marching procedure, since equations are parabolic. The maximum step-size in the streamwise direction is limited to five times the minimum size in the radial direction of the control volume. At each axial location, the thermal properties for respective control volumes, are determined from the axial pressure and temperature by using a numerical code of ref. [20].

The hydrodynamically, full-developed, isothermal circular tube flow is assumed at the starting point of the heating section. The following boundary conditions are used at the wall:

$r = 0$(center line):

$$\frac{\partial U}{r} = \frac{\partial K}{\partial r} = \frac{\partial \varepsilon}{\partial r} = \frac{\partial T}{\partial r} = \frac{\partial \overline{t^2}}{\partial r} = \frac{\partial \varepsilon_t}{\partial r} = 0$$

and

$r = D/2$(wall):

$$U = k = \varepsilon = \overline{t^2} = \varepsilon_t = 0,$$

$$\frac{\partial T}{\partial r} = \frac{q_w}{\lambda_w}(\text{constant heat flux}).$$

The computations are processed in the following order:

(1) Specify the initial values of U, k, ε, T, $\overline{t^2}$ and ε_t and assign a constant axial pressure gradient. Here, the values of U, k and ε in the hydrodynamically, fully-developed, isothermal circular tube flow are employed as the initial ones.

(2) Solve the equations of U, k, ε, T, $\overline{t^2}$ and ε_t.

(3) Repeat step 2 until the criterion of convergence is satisfied, which is set at

$$\max\left|\frac{\phi^M - \phi^{M-1}}{\phi^{M-1}_{max}}\right| < 10^{-4} \qquad (12)$$

for all the variables ϕ (U, k, ε, T, $\overline{t^2}$ and ε_t). The superscripts M and M − 1 in equation (12) indicate two successive iterations, while the subscript "max" refers to a maximum value over the entire field of iterations.

(4) Calculate new values of U, k, ε, T, $\overline{t^2}$ and ε_t by correcting the axial pressure gradient.

(5) Repeat steps 2–4 until the conversion of the streamwise flow rate is satisfied under the criterion

$$\left|\frac{\iint U_{cp}\,d\theta\,dr - \iint U_{in}\,d\theta\,dr}{\iint U_{in}\,d\theta\,dr}\right| \leqslant 10^{-5} \qquad (13)$$

and evaluate the convergent values of U, k, ε, T, $\overline{t^2}$ and ε_t. Here, U_{cp} is the axial velocity under the correction process and U_{in} is that at the inlet of the circular tube.

(6) Repeat 2–5 until x reaches the desired length, i.e. a location 150 D downstream from the inlet.

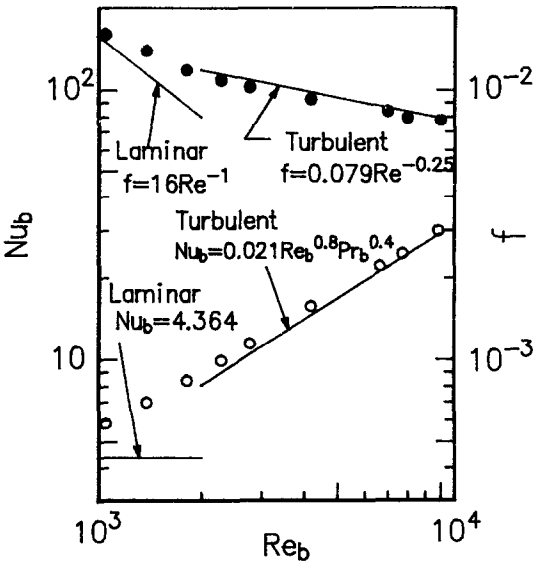

Fig. 2. Predicted Nusselt number and friction factor in the fully-developed circular tube flow for the lower heat flux case, using Model A.

In the present study, the nondimensional heat flux parameter, q^+_{in}, is employed to indicate the magnitude of heat flux at the tube wall. The range of the parameters is: non dimensional heat flux parameter, $q^+_{in} < 0.00429$; inlet Reynolds number, i.e. Reynolds number at the onset of heating, $Re_{in} = 1000$ to 10 000; inlet gas (nitrogen) temperature, $T_{in} = 273$ K. Numerical computations were performed on a NEC personal computer (32 bit).

In order to verify the k–ε turbulence and the two-equation heat-transfer models (i.e. Model A) and to determine the reliability of the computer code, heat transfer coefficients and friction factors are calculated. The model is applied to a flow in a circular tube with a low uniform wall heat flux, i.e. maximum ratio of wall surface temperature to bulk gas temperature $T_w/T_b < 1.004$. Thus, there is no effect of the variation of the gas properties on the velocity and thermal fields. Here, the calculation is done with properties set constant. A numerical result is obtained at a location 150 times the tube diameter, downstream from the inlet, where both thermally and hydrodynamically fully-developed conditions prevail.

Figure 2 illustrates both the friction factor, f and the Nusselt number, Nu_b, as a function of the Reynolds number Re_b. For comparison, Dittus and Boelter's well-known correlation [21] of turbulent heat transfer and Blasius' formula of the friction factor are shown in the figure with solid straight lines. One observes that the calculated values of both friction factor and Nusselt number are in excellent agreement with the

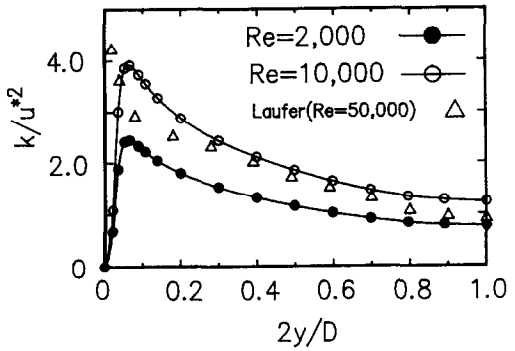

Fig. 3. A comparison of theoretical and experimental results for radial distribution of turbulent kinetic energy in the fully-developed circular tube flow for $Re = 2000$ and 10 000, using Model A.

correlations in the higher Reynolds number region, over 3000. However, Model A fails to reproduce the flow and heat transfer behavior in the lower-Reynolds number region. That is, the transition from turbulent to laminar flow is predicted to occur at a much lower Reynolds number than 2300 and the transition itself is somewhat asymptotic rather than stepwise.

Figure 3 illustrates the radial distribution of the calculated turbulent kinetic energy at $Re = 2000$ and 10 000. Here, numerical results are divided by the square of the friction velocity on the wall $(u^*)^2$. In the turbulent flow case, experimental data [22] are plotted for comparison. Model A predicts radial distribution in the turbulent flow, but it is less accurate near the wall than in the center region. One observes that although the Reynolds number is lower than the usual critical value, the turbulent kinetic energy remains. In other words, velocity fluctuations appear even in the laminar flow region. The corresponding radial distribution of the temperature variance, $\overline{t^2}$, in the thermal field is illustrated in Fig. 4. Here, it is normalized by the square of the friction temperature, t^*. The predicted $\overline{t^2}$ for $Re = 10\,000$ undergoes a sharp rise in the wall region followed by a gradual decline toward the central region. A similar distribution is observed

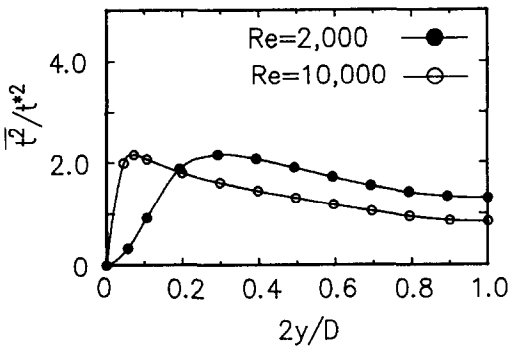

Fig. 4. Radial distributions of temperature variance in the fully-developed circular tube flow for $Re = 2000$ and 10 000, using Model A.

at $Re = 2000$, that is, temperature fluctuations never disappear in the laminar flow region.

In the above numerical results, the validity of the computer code and the accuracy for k–ε turbulence and the two-equation heat transfer models (Model A) are borne out, although the accuracy is somewhat less reliable in the transition and laminar flow (i.e. low Reynolds number) regions than in the high Reynolds number region. It is apparent that the prediction efficiency in the turbulent-to-laminar transition region is of crucial importance in the examination of the laminarization phenomena. Thus, modification to take it into account is discussed in the following.

MODIFICATION OF k–ε AND $\overline{t^2}$–ε_t MODELS

In the study of the k–ε turbulence model, Torii *et al.* [9] reported that the transition Reynolds number, from laminar to turbulent flows, is obtained by modifying the model constant, C_1 and model function f_1 in equation (11) of the original k–ε turbulence model developed by Nagano and Hishida [17]. That is, Torii *et al.* [9] proposed the value 1.44 for C_1 and the following function of the turbulent Reynolds number for f_1,

$$f_1 = 1 + 0.28 \exp\left(\frac{-R_t}{25}\right). \tag{14}$$

The same model constant and model function are used in the present study. In the following, a combination of the slightly modified k–ε turbulence model and the original two-equation heat transfer model of Nagano and Kim [14], is designated as "Model B".

To suppress the production of temperature variance in the laminar flow region, as seen in Fig. 4, more modification is made to the production terms in equation (7),

$$+ C_{P1} f_{P1} \frac{\lambda_t \varepsilon_t}{c_p \overline{t^2}} \left(\frac{\partial T}{\partial r}\right)^2 + C_{P2} f_{P2} \mu_t \frac{\varepsilon_t}{k} \left(\frac{\partial U}{\partial r}\right)^2. \tag{15}$$

This is because by the authors' preliminary examination, the radial distribution of the temperature variance was found to be substantially affected by the modification of the production terms of ε_t equation. Thus, a trial-and-error process was made to determine terms capable of simulating the behavior of temperature variance in the laminar flow region. In general, since the velocity and temperature fields are decoupled for non-buoyant flows, the velocity field can be solved first, followed by the temperature field. In other words, the change in the thermal field depends on the velocity field. In the present study, the terms proposed by Jones and Musonge [23], which adopt the velocity time scale k/ε instead of the thermal time scale $\overline{t^2}/\varepsilon_t$,

$$+ C_{P1} f_{P1} \frac{\lambda_{te}}{c_{pk}} \left(\frac{\partial T}{\partial r}\right)^2 + C_{P2} f_{P2} \mu_t \frac{\varepsilon_t}{k} \left(\frac{\partial U}{\partial r}\right)^2 \tag{16}$$

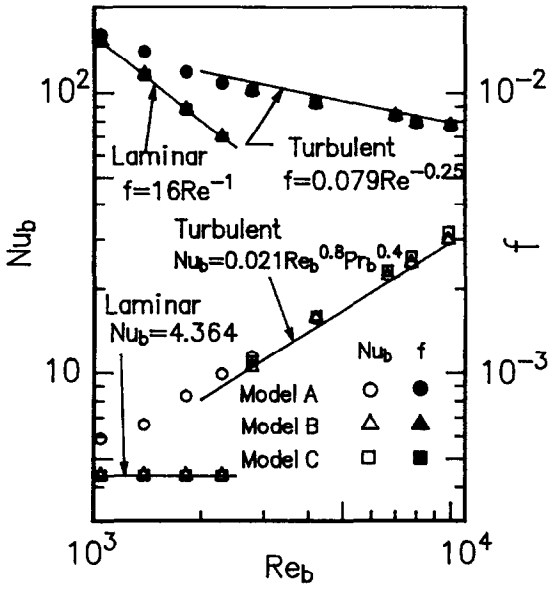

Fig. 5. Predicted Nusselt number and friction factor in the fully-developed circular tube flow for the lower heat flux case, using Models B and C.

are employed to replace equation (15). Thus, the modified transport equation of ε_t is expressed as

$$\bar{\rho}U\frac{\partial\varepsilon_t}{\partial x}+\overline{\rho\tilde{V}}\frac{\partial\varepsilon_t}{\partial r}=\frac{1}{r}\frac{\partial}{\partial r}\left\{r\left(\frac{\lambda_t}{c_p\sigma_\phi}+\frac{\lambda}{c_p}\right)\frac{\partial\varepsilon_t}{\partial r}\right\}$$

$$+C_{P1}f_{P1}\frac{\lambda_{t\varepsilon}}{c_{pk}}\left(\frac{\partial T}{\partial r}\right)^2+C_{P2}f_{P2}\mu_t\frac{\varepsilon_t}{k}\left(\frac{\partial U}{\partial r}\right)^2-C_{D1}f_{D1}\rho\frac{\varepsilon_t^2}{\bar{t}^2}$$

$$-C_{D2}f_{D2}\rho\frac{\varepsilon\varepsilon_t}{k}+\frac{\alpha\lambda_t}{c_p}(1-f_\lambda)\left(\frac{\partial^2 T}{\partial r^2}\right)^2. \quad (17)$$

Here, the model constants and model functions in equation (17), which are the same as that recommended by Nagano and Kim [14], are employed. In the following, a combination of the k–ε turbulence and two-equation heat transfer models, which are slightly modified here, is designated as "Model C".

The next step is to verify the modified models (Models B and C). The numerical results are illustrated in Fig. 5, in the same manner as Fig. 2, along with the result of Model A. Models B and C predict that the transition from turbulent to laminar flows occurs at a higher Reynolds number than that obtained by Model A. The obtained transition Reynolds number, approximately 2200, as well as the general behavior of both friction factor and Nusselt number in the transition region, are found to be much more reasonable than those predicted by Model A. When the Reynolds number is in the turbulent region, i.e. over than 2300, no substantial difference among the results obtained by Models A, B and C is recognized in friction factors. As for the heat transfer calculation, Model C predicts a higher Nusselt number than that obtained by Models A and B in the turbulent region. In other words, the numerical result obtained by

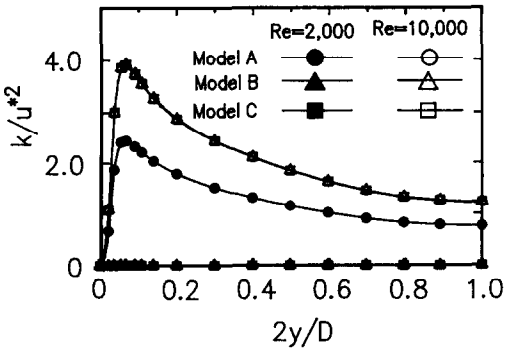

Fig. 6. Radial distributions of turbulent kinetic energy in the fully-developed circular tube flow for $Re = 2000$ and 10 000, using Models B and C.

Model C is about 10% higher than the experimental correlation. This is because for Model C, the same model constants and model functions as the original $\bar{t}^2$–ε_t heat-transfer model of Nagano and Kim [14] are used despite its modification. Thus, the task of improving the accuracy of the model in the turbulent region, i.e. modification of model constants and model functions in the $\bar{t}^2$–ε_t model, remains.

The radial distributions of calculated turbulent kinetic energy at $Re = 2000$ and 10 000 are depicted in Fig. 6, in the same form as Fig. 3, comparing the results of Models B and C with that of Model A. Lam and Bremhorst [24] suggested that the radial profiles of the turbulent kinetic energy etc. are substantially affected by the form of f_1 in equation (11). However, no such definite difference is seen among the results of the three models at $Re = 10\,000$. In the laminar flow region, i.e. for $Re = 2000$, Models B and C predict an attenuation in the turbulent kinetic energy over the whole pipe cross-section, which is a prominent contrast to that of Model A. The corresponding radial distributions of the temperature variance are illustrated in Fig. 7, in the same manner as Fig. 4. In the turbulent flow region, i.e. for $Re = 10\,000$, no difference is seen between the results of Models A and B, while both models predict a somewhat lower value than that of Model C over the pipe cross-section. It is observed that although Model B predicts a decrease in

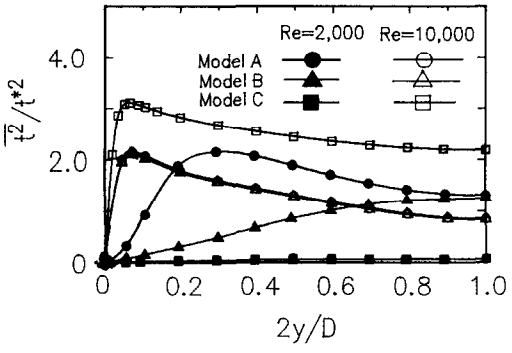

Fig. 7. Radial distributions of temperature variance in the fully-developed circular tube flow for $Re = 2000$ and 10 000, using Models B and C.

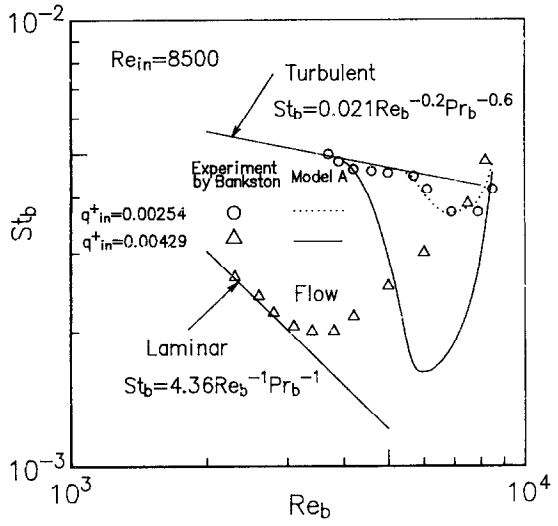

Fig. 8. Variation of the predicted local Stanton number with Reynolds number as a function of the nondimensional heat flux parameter, using Model A.

the temperature variance near the wall, an appreciable amount of temperature fluctuation remains in the laminar flow region. On the contrary, Model C reproduces a remarkable reduction in the temperature variance over the whole pipe cross-section.

It is found that: (i) the accuracy of Model A in the fully turbulent flow region is, as a whole, not affected by the above modifications, while its poor accuracy in the transition region is substantially improved; and (ii) especially, Model C reproduces the thermal transport phenomena in the laminar and transition flows in the slightly heated pipe, i.e. attenuations in both the turbulent kinetic energy and temperature variance.

RESULTS AND DISCUSSION

The local heat transfer coefficients in a strongly heated gas flow are illustrated in Fig. 8 in the form of Stanton number St_b vs Reynolds number Re_b, with q^+_{in} as the parameter, in which the numerical results of Model A are compared with the experimental data of Bankston [1]. As for the experiment, the uncertainty in the heat transfer coefficients strongly depends on the accuracy of local heat flux and inner wall temperature. That is, each test section was individually calibrated by determining the local resistivity of the tube wall and the local effective heat-exchange coefficient between the outer wall of the tube and the environment. The inner wall temperature of the tube was calculated using measured outside wall temperature, in which the uncertainty was reduced by taking into account radial and axial conductions (including the effects of temperature-dependent thermal conductivity, electrical resistivity and the diameter of the tube) and radiation from the outer surface of the tube. Although these effects were also taken into account to determine local heat flux, the streamwise distribution and the deviation level from the constant heat flux condition were not reported in literature [1]. The inlet bulk Reynolds number is fixed at 8500. Dittus–Boelter's turbulent heat transfer correlation and the Stanton number of the laminar flow heat transfer under a constant wall heat flux condition are superimposed in the figure with solid straight lines. A reduction in the bulk Reynolds number is observed along the flow, as seen in Fig. 8. This corresponds to the change in the streamwise location because the bulk Reynolds number decreases gradually from the inlet value with the axial distance as a result of an increase in molecular viscosity due to heating. It is observed that although the measured Stanton number at q^+_{in} = 0.00254 decreases in the first stage, i.e. in the thermal entrance region, subsequently, it begins to recover and approaches the turbulent correlation in the downstream part. This implies no laminarization. The streamwise variation of the Stanton number is reproduced by Model A. On the contrary, one observes for q^+_{in} = 0.00429 that the Stanton number in the experiment deviates markedly from the turbulent correlation and rapidly approaches the laminar value as the flow goes downstream. Bankston pointed out that this substantial reduction is ascribed to the occurrence of laminarization. The calculated Stanton number, however, decreases due to the thermal entrance effect, ceases to decrease after its initial drop, begins to recover and finally approaches the turbulent correlation. It is found that although Model A predicts the streamwise variation of Stanton numbers in the case of relatively low heat flux, it is of little use in investigating the laminarization phenomena of strongly heated gas flows.

Numerical results of Models B and C are illustrated in Fig. 9 in the same manner as Fig. 8, superimposed with the experimental data of Bankston [1]. Although Model B reproduces the streamwise variation of the

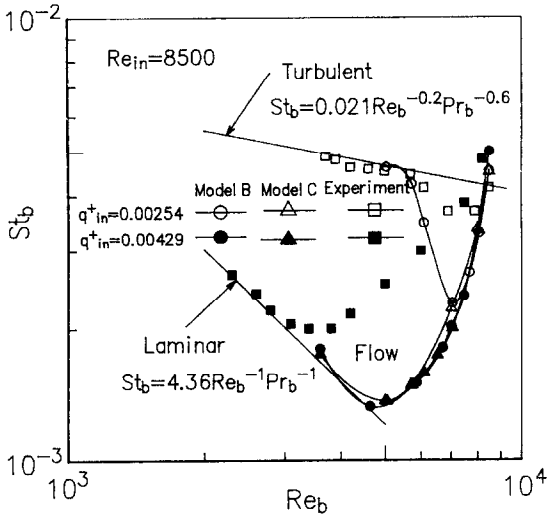

Fig. 9. Variation of the predicted local Stanton number with Reynolds number as a function of the nondimensional heat flux parameter, using Models B and C.

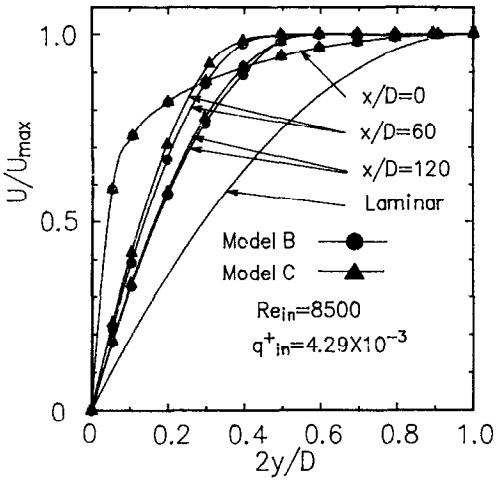

Fig. 10. Variation of time-averaged streamwise velocity profiles in laminarizing flow with three different axial locations, using Models B and C.

experimental data for $q_{in}^{+} = 0.00254$, its accuracy is somewhat inferior to that of Model A, as seen Fig. 8. In contrast, the local Stanton numbers obtained by Model C follow a pattern similar to the measured one of the laminarizing flows, even in the case of $q_{in}^{+} = 0.00254$. For $q_{in}^{+} = 0.00429$, although Models B and C cannot precisely reproduce the corresponding experimental data, both models predict a remarkable reduction in the Stanton number along the flow, which forms a prominent contrast to the case of Model A. It should be noted that the accuracy of Models B and C is somewhat inferior to that of both the k–ε model modified by Torii *et al.* [9] and the k–kL model developed by Kawamura [8], in which the turbulent Prandtl number is employed to determine the turbulent thermal diffusivity. The original $\overline{t^2}$–ε_t model used here was developed for a flat-plate thermal boundary layer, the thermal entrance region of a pipe, and the turbulent heat transfer in fluids with different Prandtl numbers, although it was not applied to the strongly heated gas flow including dependency of the gas properties on temperature as well as the change in the density. Thus, discrepancy between the experimental data and the numerical results, as seen in Fig. 9, seems to be due to the accuracy of the $\overline{t^2}$–ε_t model. It is found from the above results that Models B and C can predict the deterioration in heat transfer performance due to laminarization, although the task of improving the accuracy of both models remains. Thus, Models B and C may give detailed information on the flow structure and the thermal transport characteristics in the laminarizing flow.

An attempt is made to explore the mechanisms of the laminarizing flow based on the numerical results at $q_{in}^{+} = 0.00429$ using Models B and C. Figure 10 illustrates the radial distributions of the time-averaged streamwise velocity U/U_{max} at three different axial locations. They are normalized by the maximum value U_{max} at each axial location. The laminar flow profile is superimposed in the figure with a solid line for comparison. No substantial difference is recognized between the results of the two models at each axial location. It is observed that as the flow goes downstream, the velocity gradient at the wall is significantly diminished and approaches the laminar velocity profile. This behavior is in good agreement with the measurement by Mori and Watanabe [5] and the numerical analysis by Torii *et al.* [9, 11]. The corresponding variation of the turbulent kinetic energy along the flow is illustrated in Fig. 11. Kawamura [8] and Torii *et al.* [9, 11] investigated the change in the absolute value of the turbulent kinetic energy along the flow and the relative change, in which the turbulent kinetic energy is divided by a square of the wall friction velocity at the onset of heating and by a local friction velocity, respectively. Torii *et al.* [9, 11] reported that if laminarization occurs, relative turbulent kinetic energy as well as absolute one are substantially reduced so that a similarity in the turbulence structure is not maintained along the flow. That is, turbulent kinetic energy is diminished in the laminarizing flow. Here, the turbulent kinetic energy is normalized by a square of the wall friction velocity at each axial location. One observes that as the flow goes downstream, the turbulent kinetic energy level is greatly reduced over the whole tube cross-section. A similar result is reported by Kawamura [8] and Torii *et al.* [9]. This behavior is in accordance with the variation of the streamwise velocity distribution in Fig. 10.

The radial distributions of the time-averaged temperature at three different axial locations are depicted in Fig. 12. Here the dimensionless variable is introduced as

$$\theta^{+} = \frac{T - T_c}{T_w - T_c} \tag{18}$$

where T_w and T_c are the heated wall and the centering fluid temperatures at each axial location, respectively. Perkins and McEligot [7] measured mean temperature profiles in laminarizing flows in the entrance region,

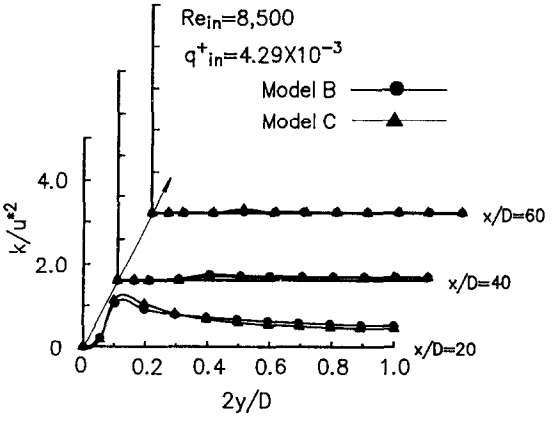

Fig. 11. Variation of turbulent kinetic energy profiles in laminarizing flow with three different axial locations, using Models B and C.

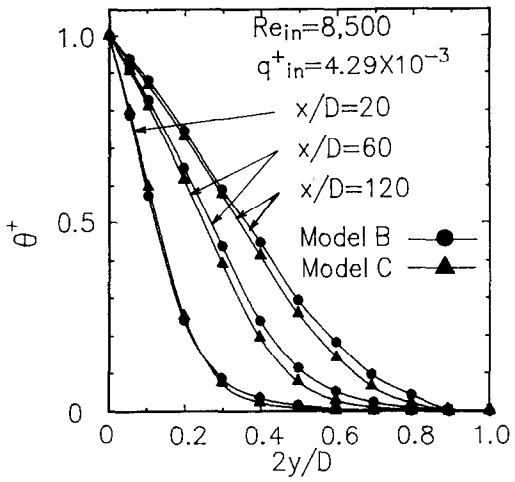

Fig. 12. Variation of time-averaged temperature profiles in laminarizing flow with three different axial locations, using Models B and C.

as mentioned previously. The inlet Reynolds number, Re_{in}, and heat flux parameter, q^{+}_{in}, are somewhat different from that employed here, i.e. $Re_{in} = 8500$ and $q^{+}_{in} = 0.00429$. In the present study, no comparison between the numerical results and the experimental data of Perkins and McEligot was made. Models B and C predict similar temperature distributions at each axial location. It is observed that the temperature gradient gradually decreases from the wall side along the flow. Figure 13 illustrates the predicted change in the turbulent heat flux profiles at three different axial locations. The turbulent heat flux level in the vicinity of the wall is substantially reduced in the flow direction. This behavior is in accordance with the variation of the time-averaged temperature distribution and causes the deterioration of the heat transfer performance, as seen in Fig. 9. Figure 14 depicts the radial distribution of the temperature variance, $\overline{t^2}$, in the thermal field at three different axial locations. Here, the temperature variance is divided

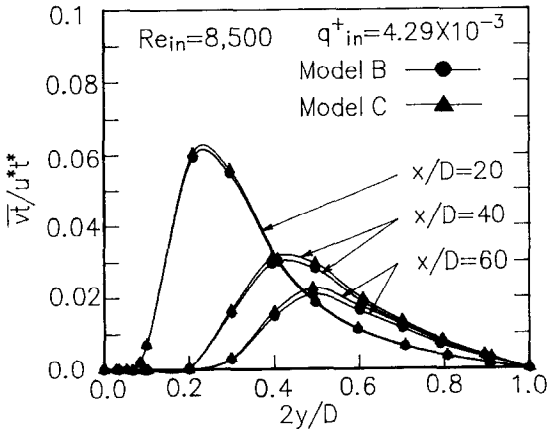

Fig. 13. Variation of turbulent heat flux profiles in laminarizing flow with three different axial locations, using Models B and C.

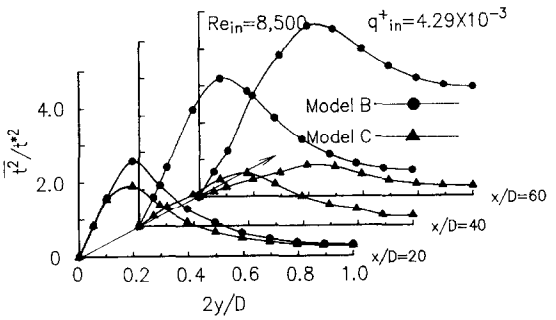

Fig. 14. Variation of temperature variance profiles in laminarizing flow with three different axial locations, using Models B and C.

by the square of the friction temperature, t^*, at each axial location. Model C predicts that as the flow moves, a reduction in $\overline{t^2}$ appears in the whole region of the flow cross-section and the peak is significantly diminished. On the contrary, however, $\overline{t^2}$ obtained by Model B is intensified over the whole pipe cross-section in the flow direction. This behavior implies enhancement in the temperature fluctuations in the thermal field. Though there is no experimental data of the temperature variance in the laminarizing flow, Ogawa *et al.* [6] observed the fluctuating temperatures in the strongly heated pipe flow at 157 D downstream with a miniaturized thermocouple and depict the oscilloscope traces in their literature. It was disclosed from the observation that as wall heat flux increases, signals corresponding to turbulent parts diminish gradually, and turbulent signals disappear entirely in the laminarizing flow case. This result is a prominent contrast to the numerical prediction of Model B, as seen in Fig. 14. However, Models B and C predict the substantial reduction in the heat transfer performance in the flow direction, as seen in Fig. 9. It is postulated that the results shown in Fig. 9 are not sensitive to $\overline{t^2}$. This will be discussed in the following. It is found that although Model B predicts the flow structure in the laminarizing flow in the strongly heated pipe, it cannot reproduce the corresponding behavior in the thermal field, i.e. an attenuation in the temperature fluctuations due to strong heating. Therefore, Model B gives no more detailed or precise information on the thermal field in investigating the laminarization phenomena.

A reduction in the temperature variance in the laminarizing flow becomes clearer by taking the budget of the temperature variance, $\overline{t^2}$. Equation (6), which governs $\overline{t^2}$, consists of four terms: molecular and turbulent diffusions, production and dissipation. The contribution of each term is depicted in Fig. 15 using Model C. In this figure, (a) and (b) correspond to the results at the 20 and 60 diameter downstream locations, respectively. The molecular diffusion term is seen to become more significant in the central region at $x/D = 60$ than at $x/D = 20$. In contrast, the role of the turbulent diffusion term is reduced at $x/D = 60$. It is observed that in the downstream region, production

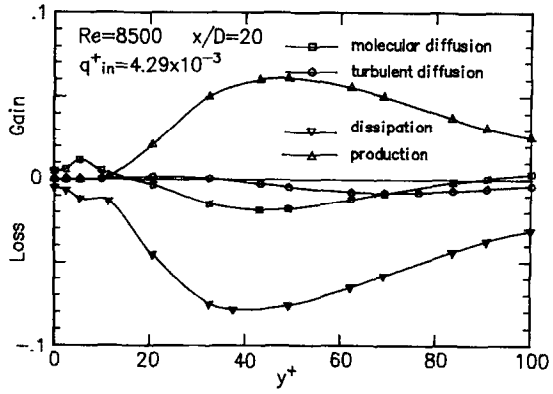

(a)

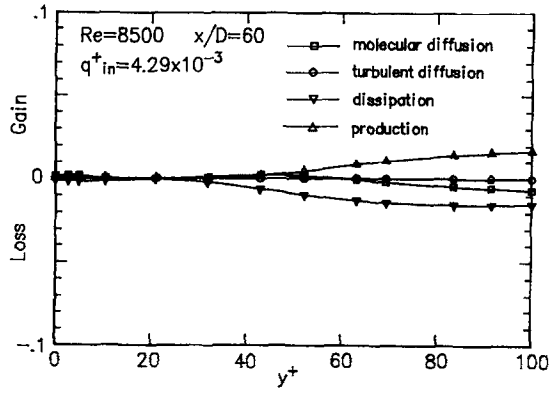

(b)

Fig. 15. The budget of temperature variance in laminarizing flow, using Model C, at: (a) $x/D = 20$; and (b) $x/D = 60$.

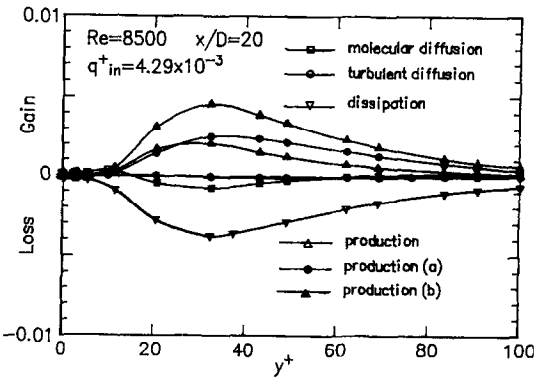

(a)

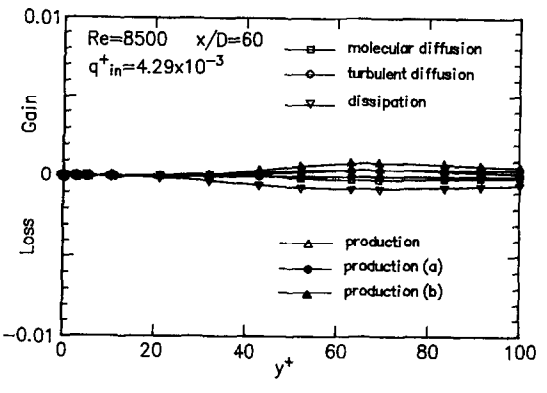

(b)

Fig. 16. The budget of the dissipation rate of temperature variance in laminarizing flow, using Model C, at: (a) $x/D = 20$; and (b) $x/D = 60$.

and dissipation terms are substantially diminished over the entire flow region. The remarkable reduction in the production of $\overline{t^2}$ is ascribed to a decrease in the temperature gradient at the wall, as seen in Fig. 12. The attenuation in the dissipation of $\overline{t^2}$ becomes clearer in Fig. 16 by taking the budget of ε_t. In this figure, (a) and (b) correspond to the results at the 20 and 60 diameter downstream locations, respectively. Production is the sum of production (a) and production (b) in Fig. 16. Both terms mean production due to time-averaged temperature and mean shear, which correspond to the second and third terms in the right side of equation (17), respectively. One observes that each term is substantially attenuated over the entire flow region in the flow direction. The substantial decrease in the production of ε_t is ascribed to a drastic reduction in both productions (a) and (b). That is, the production of ε_t is suppressed by reductions in time-averaged temperature and time-averaged velocity gradients, as seen in Figs. 10 and 12. It results in an attenuation in the dissipation of $\overline{t^2}$, as seen in Fig. 15.

Since the eddy diffusivity concept is employed to determine the turbulent heat flux, $-c_p\bar{\rho}\,\overline{vt}$, in equation (2), it is directly related to k, ε, $\overline{t^2}$ and ε_t through equation (4) and (5), and is rewritten as

$$-\overline{vt} = C_t f_t \frac{k^2}{\varepsilon}\sqrt{2R}\frac{\partial T}{\partial r}. \tag{19}$$

Now, $-\overline{vt}$ is shown to be dependent upon k, ε and the time-scale ratio, R. Figure 17 shows the predicted radial distributions of the velocity dissipation time scale, τ_u, the temperature dissipation time scale, τ_t, and their ratio, R, at three different axial locations. It is observed that both time scales increase monotonically with an increase in the distance from the wall and τ_u is always larger than τ_t. In other words, the temperature fluctuation dissipates faster than the velocity fluctuation except near the heating wall. These time scale characteristics are in accord with the DNS data of Kasagi *et al.* [25]. A similar trend is observed even in the strongly heated laminarizing gas flow, where τ_u and τ_t are simultaneously induced along the flow. On the contrary, only a slight change in the time-scale ratio appears. It is observed in Figs. 9 and 14 that the heat transfer performance in the laminarizing flow is diminished despite an increase or a decrease in the temperature variance along the flow. Equation (19) implies that the turbulent heat flux is extremely

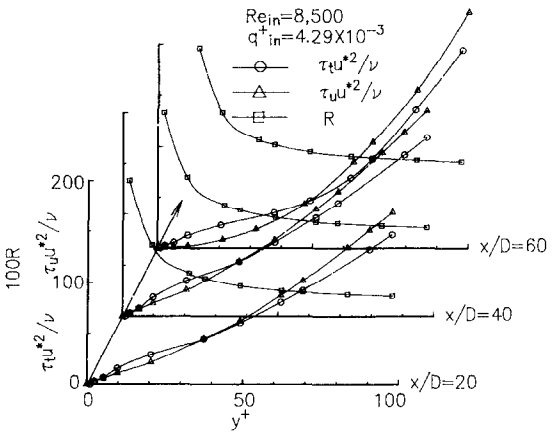

Fig. 17. Variation of radial distributions of the velocity dissipation time scale, the temperature dissipation time scale and their ratio in laminarizing flow with three different axial locations using Model C.

affected by the turbulent kinetic energy, although the time scale ratio, R, also depends on the change in the temperature variance. Therefore, a reduction in the turbulent kinetic energy, as seen in Fig. 11, causes both an attenuation in the predicted local Stanton number, i.e. a deterioration in the turbulent heat flux and a reduction in time-averaged temperature gradient at the wall even if the temperature variance is somewhat increased or decreased. In other words, as for Model C, modification of the $\overline{t^2}-\varepsilon_t$ heat transfer model, i.e. the effect of the time scale, k/ε, changed from $\overline{t^2}/\varepsilon_t$ in the production term of the original ε_t equation is to cause a decrease in the temperature variance in the laminarizing flow.

SUMMARY

A $\overline{t^2}-\varepsilon_t$ heat-transfer model and a k–ε turbulence model have been employed to numerically investigate fluid flow and heat transfer in a strongly heated circular tube. Consideration is given to the streamwise variation of the flow and thermal fields in the laminarizing flow. The results are summarized here.

(1) The modified model, in which an empirical constant and a model function in the original ε equation are slightly modified and the production term proposed by Jones and Musonge is employed to replace that of the original ε_t equation, can precisely reproduce the thermal and fluid flow characteristics in the laminar and transition regions. In the high Reynolds number region, the modification shows a slight effect on the accuracy.

(2) For $q_{in}^{+} = 0.00429$, the modified model predicts the substantial reduction in the local Stanton number in the strongly heated gas flow, although it cannot precisely reproduce the corresponding experimental data of Bankston [1]. In the lower heat flux case, in which no laminarization occurs, the modified model reproduces the streamwise variation of the Stanton number no more exactly than the original model.

(3) When laminarization takes place, the velocity gradient in the vicinity of the wall is decreased along the flow, resulting in a substantial attenuation in the turbulent kinetic energy over the entire tube cross-section. At the same time, the temperature variance and the turbulent heat flux are also diminished over the whole tube cross-section in the flow direction and it results in a decrease in time-averaged temperature gradient at the wall.

(4) Although both the velocity and temperature dissipation time scales are substantially amplified in the laminarizing flow, their ratio is slightly increased.

(5) The temperature fluctuation dissipates faster than the velocity fluctuation, even if the flow is laminarized.

(6) Consequently, the turbulent heat flux is diminished by a decrease in the turbulent kinetic energy over the pipe cross section, resulting in the deterioration of heat transfer performance.

Although the modified model proposed here deepens our insight into the laminarization phenomena due to strong heating, further study must be made to improve the model itself in order to achieve sufficient prediction accuracy.

REFERENCES

1. Bankston, C. A., The transition from turbulent to laminar gas flow in a heated pipe. *Transactions of ASME, Series C*, 1970, **92**, 569–579.
2. Coon, C. W. and Perkins, H. C., Transition from the turbulent to the laminar regime for internal convective flow with large property variations. *Transactions of ASME Series C*, 1970, **92**, 506–512.
3. McEligot, D. M., Coon, C. M. and Perkins, H. C., Relaminarization in tubes. *International Journal of Heat and Mass Transfer*, 1970, **13**, 431–433.
4. Perkins, K. R., Schade, K. W., and McEligot, D. M., Heated laminarizing gas flow in a square duct. *International Journal of Heat and Mass Transfer*, 1973, **16**, 897–916.
5. Mori, Y. and Watanabe, K., Reduction in heated transfer performance due to high heat flux. *Transactions of the Japanese Society for Mechanical Engineers*, 1979, **45**, 397, 1343–1353 (in Japanese).
6. Ogawa, M., Kawamura, H., Takizuka, T. and Akino, H., Experiment on laminarization of strongly heated gas flow in vertical circular tube. *Journal of Atomic Energy Society of Japan*, 1982, **24**, 60–67 (in Japanese).
7. Perkins, K. R. and McEligot, D. M., Mean temperature profiles in heated laminarizing air flows. *Transaction of ASME, Series C*, 1975, **97**, 589–593.
8. Kawamura, H., Prediction of strongly heated turbulent flow of gas in a circular tube using a two-equation model of turbulence. *Transactions of the Japanese Society of Mechanical Engineers*, 1979, **45**, 1038–1046 (in Japanese).
9. Torii, S., Shimizu, A., Hasegawa, S. and Higasa, M., Laminarization of strongly heated gas flows in a circular tube (numerical analysis by means of modified k–ε model). *JSME International Journal, Series, II*, 1990, **33**, 538–547.
10. Fujii, S., Akino, N., Hishida, M., Kawamura, H. and Sanokawa, K., Numerical studies on laminarization of

heated turbulent gas flow in annular duct. *Journal of Atomic Energy Society of Japan*, 1991, **33,** 1180–1190 (in Japanese).
11. Torii, S., Shimizu, A. and Hasegawa, S., Numerical analysis of laminarizing tube flows by means of a Reynolds stress turbulence mode. *Heat Transfer—Japanese Research*, 1993, **22,** 154–170.
12. Launder, B. E. and Shima, N., Second-moment closure for the near-wall sublayer : development and application. *AIAA Journal*, 1989, **27,** 1319–1325.
13. Koshizula, S., Takano, N. and Oka, Y., Numerical analysis of deterioration phenomena in heat transfer to supercritical water. *International Journal of Heat and Mass Transfer*, 1995, **38,** 3077–3084.
14. Nagano, Y. and Kim, C., A two-equation model for heat transport in wall turbulent shear flows. *Journal of Heat Transfer*, 1988, **110,** 583–589.
15. Youssef, M. S., Nagano, Y. and Tagawa, M., A two-equation heat transfer model for predicting turbulent thermal fields under arbitrary wall thermal conditions. *International Journal of Heat and Mass Transfer*, 1972, **35,** 3095–3104.
16. Sommer, T. P., So, R. M. C. and Lai, Y. G., A near-wall two-equation model for turbulent heat fluxes. *International Journal of Heat and Mass Transfer*, 1992, **35,** 3375–3387.
17. Nagano, Y. and Hishida, M., Improved form of the k–ε model for wall turbulent shear flows. *Transactions of ASME, Series D*, 1987, **109,** 156–160.
18. Rodi, W., Examples of turbulence models for incompressible flows, *AIAA, Journal*, 1982, **20,** 872–879.
19. Patankar, S. V., *Numerical Heat Transfer and Fluid Flow*. Hemisphere, Washington, D.C., 1980.
20. Propath Group, Propath: a program package for thermophysical property, version 4.1, 1987.
21. McAdams, W. H., *Heat Transfer*. McGraw-Hill, New York, 1954.
22. Laufer, J., The structure of turbulence in fully developed pipe flow. NACA Report 1174, 1953.
23. Jones, W. P. and Musonge, P., Closure of the Reynolds stress and scalar flux equations. *Physics Fluids*, 1988, **31,** 3589–3605.
24. Lam, C. K. G. and Bremhost, K., A modified from of the k–ε model for predicting wall turbulence, *ASME, Journal of Fluids and Engineering*, 1981, **103,** 456–460.
25. Kasagi, N., Tomita, Y. and Kuroda, A., Direct numerical simulation of passive scalar field in a turbulent channel flow. *Journal of Heat Transfer*, 1992, **114,** 598–606.